Imaging Modalities in Brain Tumors

2

Antonios Drevelegas and Nickolas Papanikolaou

Contents

2.1 Introduction 13
2.2 Computed Tomography 13
2.3 Magnetic Resonance Imaging 15
References 32

2.1 Introduction

Imaging plays an important role in the evaluation of patients with brain tumors. CT and MRI represent the two most important and commonly used imaging modalities. They have a significant impact on patient care. The technical improvement of CT and MRI, the utility of contrast material in the imaging of brain tumors as well as the introduction of new imaging techniques, improved significantly the detection and the evaluation of brain neoplasms.

Once a brain tumor is clinically suspected, radiologic evaluation is required to determine the location, the extent of the tumor and its relationship to the surrounding structures.

This information is very important and critical in deciding between the different forms of therapy such as surgery, radiation, and chemotherapy.

In this chapter we will give an overview of the role of CT and MRI in the diagnosis of brain tumors. New imaging techniques that evaluate tissue blood flow (perfusion imaging), water motion (diffusion imaging), brain metabolites (Proton magnetic resonance spectroscopy) and blood oxygen level dependent (BOLD) imaging have also been included.

2.2 Computed Tomography

Computed tomography (CT) was introduced in the clinical practice in 1972 and rapidly became a very important factor in the radiological diagnosis. With the advent of CT in neuroradwiology direct images of the brain could be produced, and a new era in cerebral studies started. CT of the brain, which became the procedure of choice for evaluation and diagnosis of brain tumors, has

A. Drevelegas (✉)
Department of Radiology,
Aristotle University of Thessaloniki,
Thessaloniki, Greece
e-mail: adrev@med.auth.gr

N. Papanikolaou
Department of Radiology,
University Hospital of Heraklion,
Medical School of Crete,
Greece

A. Drevelegas (ed.), *Imaging of Brain Tumors with Histological Correlations*,
DOI: 10.1007/978-3-540-87650-2_2, © Springer-Verlag Berlin Heidelberg 2011

replaced invasive procedures such as pneumoencephalography or cerebral angiography. Progressive improvement of the image quality, reduction of costs, and reduction of scan times has resulted in significant expansion of CT applications. The utility of contrast material in the imaging of the brain improved the efficacy of CT in the diagnosis of brain tumors. Enhancement is the increased difference in an imaging characteristic between a lesion and surrounding normal tissue after administration of contrast agent. This is due to the disruption of the blood–brain barrier (BBB) of the tumor vessels, which permits the passage of the contrast material into the extracellular spaces of the tumor (Fig. 2.1). On CT, the increased concentration of the contrast material within the tumor interstitium results in higher attenuation values within the tumor than in the surrounding brain. The majority of the brain tumors enhance after the administration of contrast material. The enhancement characteristics of different types of brain tumors will be discussed in the following chapters.

Progress in CT development continued rapidly and new technology has revolutionized the field. Spiral and multislice CT allow faster acquisition times with substantially improved 3D spatial resolution. CT angiography provides images of excellent quality in a noninvasive way and is of great importance in the assessment of the relationship between the tumor and the vessels. Perfusion imaging techniques enable accurate measurement of CBV and CBF values in a variety of clinical and experimental settings [1].

CT-guided stereotactic biopsy is a reliable method for histological diagnosis of brain tumors and showed to be valuable in planning the appropriate treatment for each patient.

Although MR is the main diagnostic tool for diseases of the central nervous system, CT is still a valuable modality in the imaging of brain tumors. CT is superior in detecting calcification, hemorrhage, and in evaluating bone changes related to a tumor (Fig. 2.2). Patients with pacemakers or metallic devices as well as critically ill, pediatric or unstable patients represent some of the specific areas where CT is the diagnostic modality of choice [2].

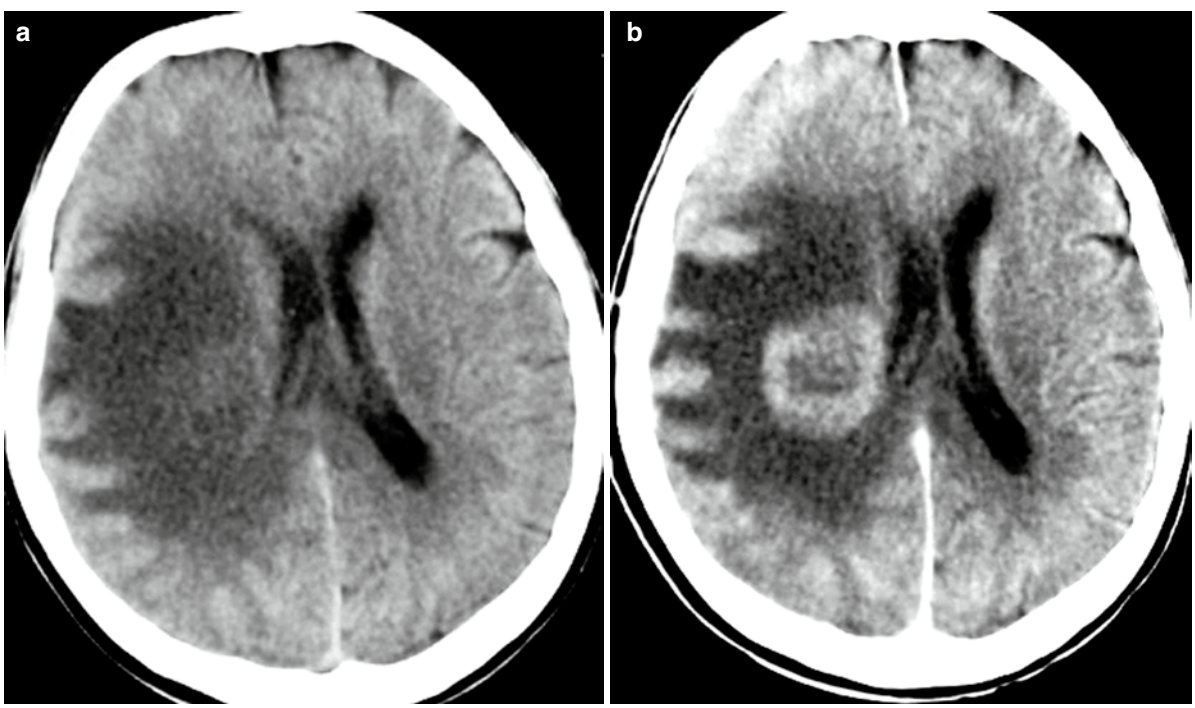

Fig. 2.1 Enhancement of tumor after IV contrast administration. (**a**) CT before and (**b**) after contrast administration. The neoplasm is clearly demonstrated on post-contrast CT. The contrast material identifies areas of BBB disruption facilitating the detection of the neoplastic tissue

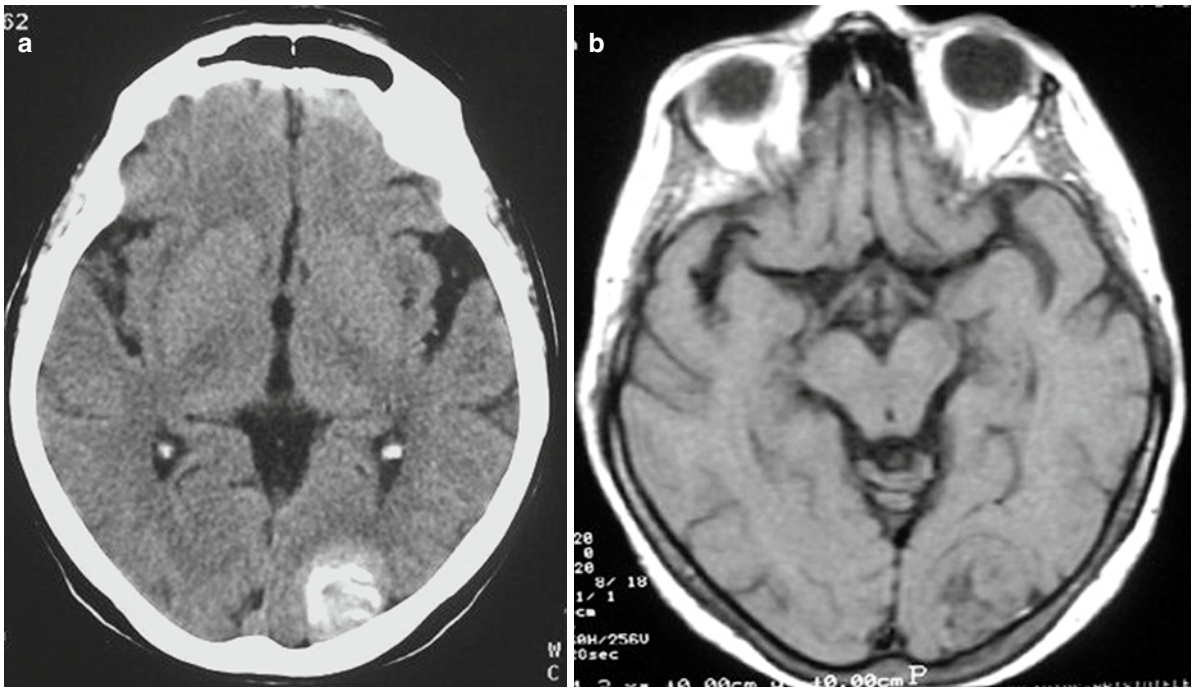

Fig. 2.2 CT versus MRI in calcified meningioma. (**a**) Axial CT. (**b**) Axial T1-weighted MRI. Densely calcified tumor is clearly demonstrated on CT. Most calcification is isointense to brain on T1WI

2.3 Magnetic Resonance Imaging

Magnetic resonance imaging (MRI) is the modality of choice for evaluating patients who have symptoms and signs suggesting a brain tumor. Its multiplanar capability superior contrast resolution and flexible protocols allow it to play an important role in assessing tumor location and extent, in directing biopsies, in planning the proper therapy, and in evaluating the therapeutic results.

The standard protocol most commonly used between institutions includes: spin-echo T1-weighted image (T1WI), proton density-weighted image (PDWI), T2-weighted image (T2WI), and T1WI after the administration of paramagnetic agent.

Most brain tumors have prolonged T1 and T2 relaxation times and appear hypointense relative to normal brain on T1WI and hyperintense on T2WI. On PDWI the tumors show intermediate hyperintensity. However, the presence of fat, hemorrhage, necrosis, and calcification are responsible for the heterogeneous appearance of some tumors. As in CT, the utility of contrast material in MRI facilitates the detection of many brain tumors and can help distinguish some tumors from the adjacent normal brain parenchyma. The MRI contrast agents most commonly used for central nervous system (CNS) tumor imaging are gadolinium (Gd) chelates. Although in normal brain Gd cannot pass from intravascular compartment to the interstitial space, in brain tumors, where the normal BBB may be disrupted, Gd is accumulated into the extracellular space of the tumor. As result in post-contrast T1WI the tumor becomes brighter than the surrounding normal brain tissue due to the shortening of T1 relaxation time. However, histologic examination of samples obtained of patients with brain tumors showed that there are regions with tumor cells outside the Gd-enhancing area.

The accepted standard dose for Gd is 0.1 mmol/kg and has proved to be valuable in the evaluation of CNS tumors (deletion). In an attempt to improve the delineation of the extent of primary brain tumors as accurately as possible to guide potential surgical or radiation therapy, several studies have been performed and have shown that the administration of higher doses of contrast agent improved significantly the enhancement of most intracranial tumors [3–7] (Fig. 2.3). This has important therapeutic implications because the zone of glioma cells delineated by enhancement after high-dose Gd likely is a better estimate of microscopic tumor extent [8].

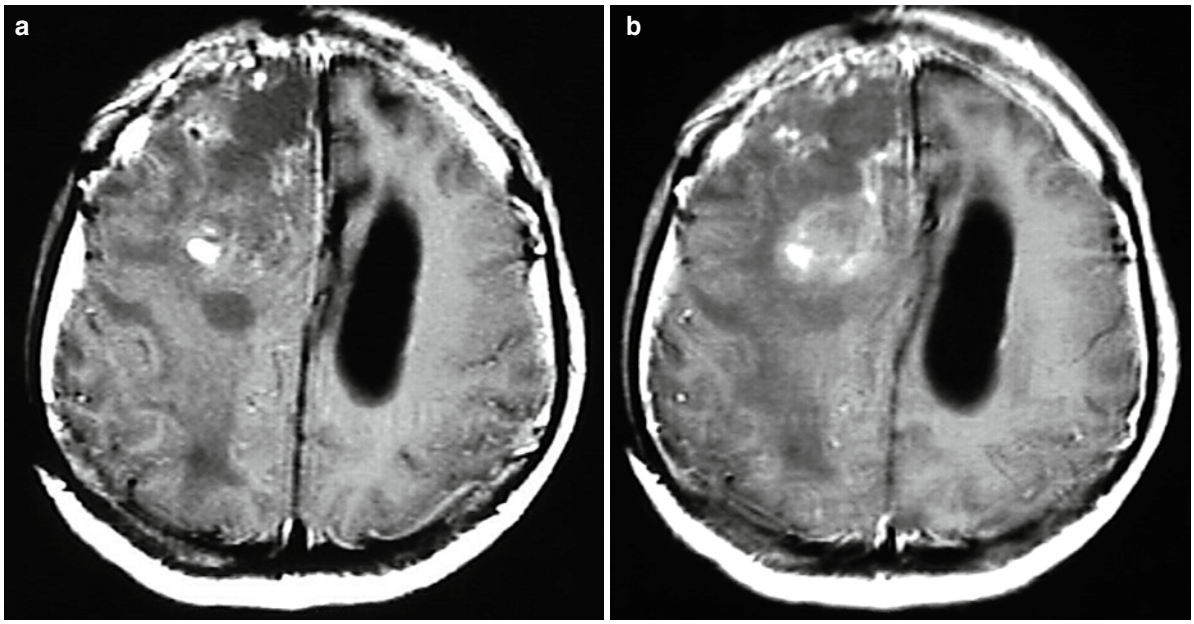

Fig. 2.3 Comparison of standard and high dose contrast material. (**a**) T1WI after administration of 0.1 mmol/kg Gd shows a ring-like enhanced tumor in the right parietal lobe. (**b**) After high dose of Gd. the ring-like enhancement of the tumor tissue is thicker and sharper

In brain metastases better lesion delineation and increase in the number of visible metastases is achieved by using double or triple doses of Gd [4, 9].

However, increasing the dose of contrast medium unfortunately increases imaging costs. In order to minimize the cost of the contrast agent, new sequences have been introduced as the standard dose magnetization transfer (MT) T1-weighted imaging which is equally effective as the triple dose T1-weighted imaging in terms of lesions conspicuity and detectability (Fig. 2.4). This magnetization transfer T1-weighted sequence is generated by suppressing the signal of the (nonenhancing) background tissue either by applying an off-resonance radio frequency (RF) prepulse or binomial on-resonance pulseto preferentially saturate bounded protons, which then transfer magnetization to mobile free protons. As a result, the signal of the white matter will be reduced since an increased amount of bounded protons in the myelin is present while the signal of pathologic tissue, containing more free protons, will remain unchanged; therefore, it will be presented with higher conspicuity [10]. In tumors MT improves the accuracy of tumor classification and allows differentiation between low-grade astrocytomas, hemangioblastomas and craniopharyngiomas [11]. In addition, MT T1WIs may be used in postoperative patients to define enhancing residual tumor not seen on standard T1WIs. A drawback of MT images is the lower sensitivity in depicting cerebral edema. As information regarding edema is much more readily available on T2WIs, we do not consider this a major disadvantage of the MT T1WIs [10].

Although the traditional spin-echo MR sequences in conjunction with the post-contrast MRI are clearly effective in detecting and delineating brain neoplasms, an additional number of MR techniques have been applied in an attempt to improve the diagnostic efficacy for tumor imaging both before and after treatment. These MR techniques may ultimately supplant conventional MR spin-echo imaging and are designed to produce a high level of contrast (instead of a certain contrast) and improved image quality and data acquisition. They are fast spin echo (FSE), inversion recovery (IR), short tau inversion recovery (STIR), fluid attenuated inversion recovery (FLAIR), gradient echo pulse sequences, and echo-planar imaging (EPI).

FSE is a spin-echo pulse sequence but with scan times shorter than the conventional spin echo. Since the scan time is greatly reduced FSE sequence allows greater patient throughout, which may be critical in clinical practice. FSE imaging is equal to SE imaging in the detection of white matter lesions larger than 5 mm

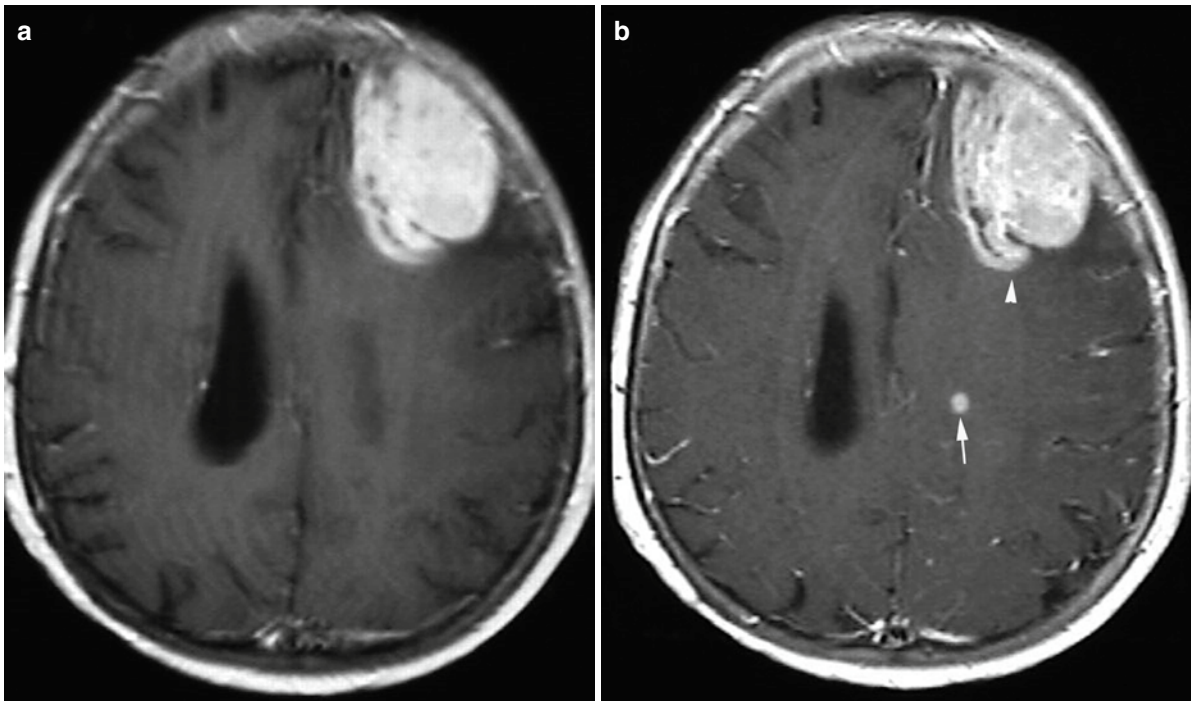

Fig. 2.4 Effect of MT image on the detection of brain metastasis. (**a**) Post-contrast T1WI shows a large enhancing lesion. (**b**) MT image shows an additional small lesion (*arrow*). Note also that MT image clearly delineates the contour of the lesion (*arrowhead*)

and is slightly less sensitive in the detection of smaller than 5 mm lesions [12]. Thus FSE sequence offers a faster alternative to conventional spin-echo in routine MRI of the brain. There are some differences between FSE and conventional SE images in terms of contrast, and these can be summarized into: (a) brighter fat appearance due to J coupling effects, (b) increased MT effects that result in darker appearance of normal white matter, and (c) less sensitivity to hemorrhagic lesions due to the presence of multiple refocusing pulses.

IR is a pulse sequence that begins with a 180° inverting pulse followed by a 90° excitation pulse, and by a 180° refocusing pulse. IR can be used to produce heavily T1WIs to demonstrate anatomy. In IR images the white matter has a short T1 and appears white, the gray matter has a longer T1 and appears gray and the cerebrospinal fluid has a very long T1 and appears dark. This sequence provides an excellent gray–white matter contrast, which is important in localization and assessing mass effects (Fig. 2.5).

STIR is an IR sequence with a short inversion time ranging from 130 to 200 ms depending on the field strength and is used to achieve suppression of the fat signal in a T1WI. Spin preparation not only eliminates the signal from fat, it also adds inverted T1 contrast to the image. Tissue with a long T1 appears brighter than tissue with short T1. STIR should not be used in conjunction with contrast because the signal from the enhancing tissue may be nulled.

FLAIR imaging is another variation of the IR sequence with an inversion time ranging from 2,000 to 2,500 ms and may be used to suppress the high CSF signal in T2- and proton density-weighted images so that the pathology adjacent to the CSF is seen more clearly. The suppression of the CSF signal is achieved by applying an inversion pulse with a long recovery time between this pulse and the start of the measurement. With this sequence, CSF artifacts are reduced and heavily T2WIs are obtained with a long echo time. FLAIR images enable better delineation of the lesions adjacent to the ventricles. Additionally, subtle lesions near the cortex stand out against a background of attenuated CSF [13].

FLAIR images provide better definition between edema and tumor. Cerebral edema associated with brain tumors is also better delineated on FLAIR image. Therefore, they may be used as an adjunct to T2-weighted or proton density-weighted spin-echo

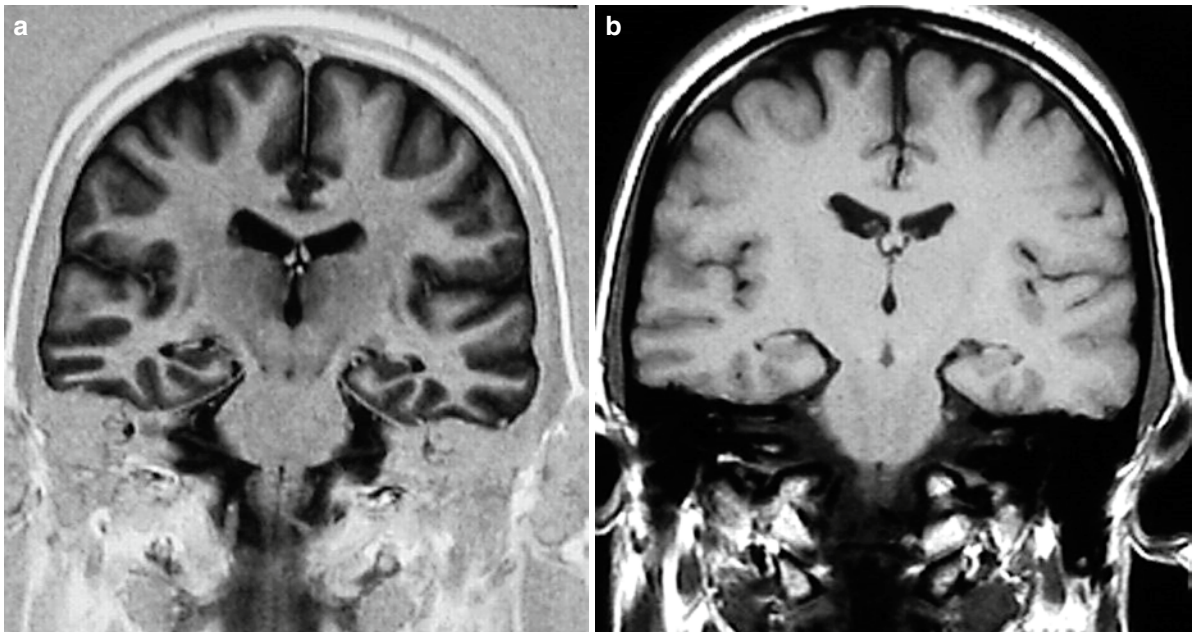

Fig. 2.5 The contrast between gray and white matter is significantly improved on the coronal inversion recovery image (**a**) compared to the conventional T1-weighted spin-echo image (**b**)

images [14]. Contrast-enhanced FLAIR MR imaging has been successfully used by taking advantage of the T1 effect to achieve a particularly high contrast between tumor and background tissue [15]. They allow an exact delineation of enhancing and nonenhancing tumor parts in one sequence (Fig. 2.6). Although FLAIR technique is simple to implement, its disadvantages include long imaging times and a limited number of sections.

In gradient echo pulse sequence the 180° refocusing pulse is omitted and a flip angle other than 90° is used. After the RF pulse is withdrawn, the free induction decay (FID) signal is immediately produced due to inhomogeneities in the magnetic field and T2* dephasing occurs. The magnetic moments within the transverse component of magnetization dephase, and are then rephased by a gradient .The gradient rephases the magnetic moments so that a signal can be received by the coil, which contains T1 and T2 information and is called gradient echo [16].

In gradient echo pulse sequence, the repetition time (TR) is reduced due to the absence of 180° rephasing pulse. The TR can also be reduced because flip angles other than 90° can be used. As a consequence, the imaging time is reduced and the motion artifacts are decreased. Therefore, gradient echo pulse sequences (instead of they) can be valuable for examining critically ill, anxious or uncooperative patients whose conventional or fast spin-echo images show considerable motion artifacts [17]. Gradient echo images are very sensitive to flow, produce angiographic types of images, and may be used to clarify focal or linear regions of signal void within a mass whether they represent dense calcification or flow within tumor vessels. Calcified neoplasms in gradient-echo images appear as focal regions of signal void, while intratumoral vessels appear as round or linear areas of high signal intensity. Gradient echo pulse sequences are also very sensitive in the detection of hemorrhage. They are also particularly suited to 3D imaging, which is used when high resolution and thin contiguous slices are required. 2D and 3D GRE sequences are essential for time-of-flight MR angiography (MRA). The most important disadvantage is that there is no compensation for magnetic field inhomogeneities, and therefore, they are very sensitive to magnetic susceptibility artifacts.

The steady state is a GE pulse sequence where the TR is shorter than the T1 and T2 times in tissues. In the steady-state sequence coexist both the longitudinal and the transverse magnetizations. Fast imaging with steady precession (FISP) and constructive interference of steady state (CISS) are steady-state gradient-echo techniques that produce heavy T2-weighting images. The

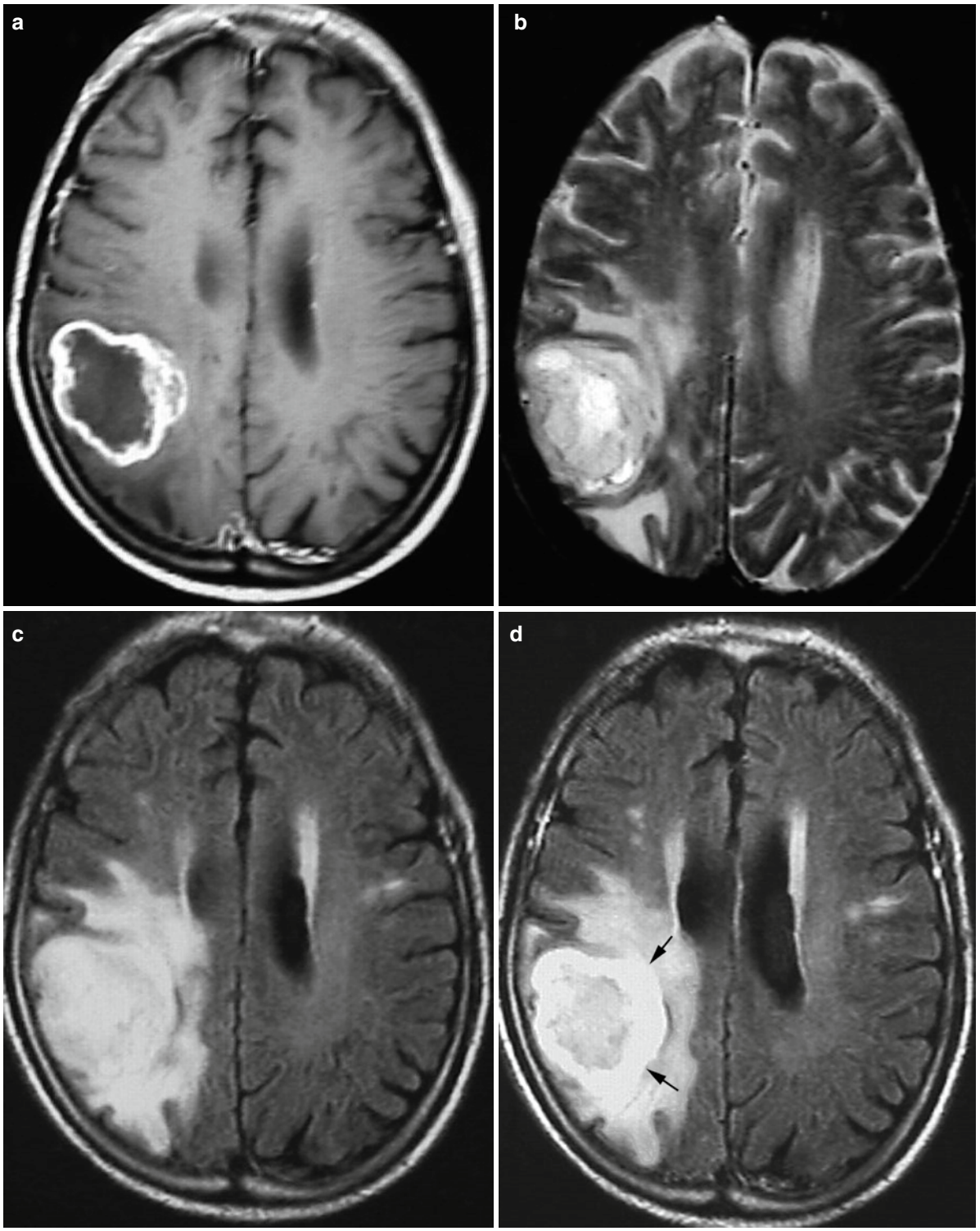

Fig. 2.6 Left parietal glioblastoma. (**a**) Post-contrast T1WI shows an irregular ring-like enhancement. (**b**) T2WI shows a high signal mass surrounded by peritumoral edema (**c**) FLAIR image shows the mass and the peritumoral edema which is more prominent than on T2WI (**d**). Post-contrast FLAIR image clearly demonstrates the ring-like enhanced tumor (*arrows*) as well as the surrounding edema

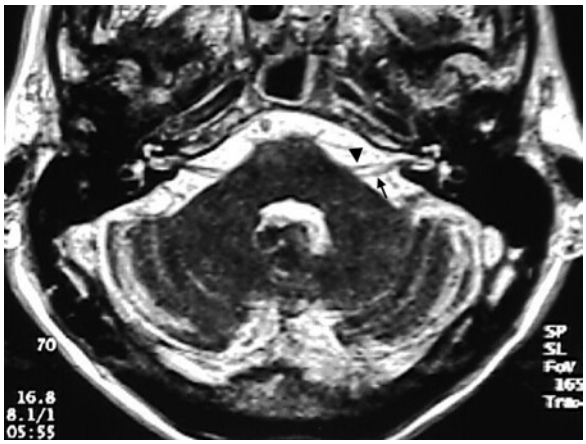

Fig. 2.7 Axial 3D CISS image shows clearly the facial (*arrowhead*) and the vestibular nerve (*arrow*)

CISS sequence is used for the imaging of basal cisterns and/or the discrimination of the facial-vestibulocochlear nerve complex [4] (Fig. 2.7).

EPI is the fastest MR imaging technique and is achieved by means of rapid gradient switching, which maps all phase and frequency points in K-space during a single echo period. It allows one to collect all the data required to reconstruct an image from a single RF excitation. Individual images may be acquired on the order of 50–100 ms and so an entire brain survey can be completed in as little as 1 s. To keep the total time for data collection brief, gradients with high slew rate are used. In EPI can be used any combination of RF pulses used in conventional spin-echo technique. Alternatively a T2*-dependent gradient echo imaging can be applied (GRE EPI).

An echo-planar image can be obtained either with a single-shot technique, where all data are collected after one excitation or with a multi-shot technique in which K-space is broken up into several sections and each section is scanned during subsequent TRs. With single-shot EPI a study of the entire brain can be performed in as little as 2 s [18, 19]. However, the sensitivity of single-shot EPI is lower compared with proton-density and T2-weighted conventional spin-echo imaging for the detection of small brain lesions. Multi-shot EPI proved to be superior to single shot echo planar sequences in terms of lesion conspicuity and delineation [20].

In a study single-shot EPI depicted up to 70% of multiple sclerosis lesions larger than 1cm and only 23% of smaller lesions (<5 mm) [21]. When multi-shot echo-planar technique is used, the sensitivity for lesion detection increases to 98% for lesions larger than 1cm and 77% for lesions smaller than 5 mm. Despite the increased spatial resolution provided with multi-shot technique, EPI is still suffering from decreased spatial resolution, poor fat suppression, and increased ghosting and susceptibility artifacts (signal loss and geometric distortion). Therefore, conventional spin-echo or fast spin-echo imaging remains the preferred imaging technique. However, the greater sensitivity of echo-planar images to magnetic susceptibility variations makes them more sensitive to small amounts of hemorrhage in tissue. In addition, EPI reduces imaging time and motion artifacts allowing the MR examination of uncooperative claustrophobic and pediatric patients.

An alternative approach to the use of EPI sequences is to combine EPI and FSE techniques to produce a combined gradient-echo (GRASE) image. The GRASE sequence produces reasonable quality T2WIs. At present, GRASE does not provide the image quality and contrast spectrum of conventional or fast spin-echo sequences; nevertheless, it might be useful for uncooperative patients whose conventional or spin-echo sequences show considerable motion artifacts [17].

The combination of half-Fourier acquisition and single-shot turbo spin-echo (HASTE) offers also a rapid imaging technique. This sequence is T2-weighted and is excellent for rapid screening of the brain.

The introduction of EPI and other subsecond imaging techniques has allowed the fast progression of functional MR imaging (fMRI). Diffusion, perfusion, and BOLD functional MR imaging allows a better understanding of pathophysiology of various pathologic states. Cerebral ischemia, brain tumors, multiple sclerosis, metabolic diseases, and neurocognitive disorders represent a spectrum of diseases where fMRI provides useful diagnostic information and may allow better monitoring of the effects of therapy.

Diffusion-weighted imaging is a unique tissue contrast technique based on the diffusion of water molecules, which move along random pathways (Brownian motion). Usually a spin-echo EPI sequence is utilized for DWI, where a pair of identical gradient pulses is added before and after the application of the refocusing pulse. The physical principle behind DWI is analogous to that of phase contrast MRA, although PCA is referred to macroscopic motion while DWI is referred to microscopic motion. More specifically, the first gradient pulse induces phase shifts to water molecules

while the second gradient cancels the phase shifts by fully rephasing the spins. Moving molecules will acquire a phase shift due to their motion during the time interval in between the application of diffusion gradients. In other words, stationary spins will be fully refocused that means no phase shifts, while moving spins will be partially refocused that means a specific amount of phase shift that causes signal loss.

The signal amplitude for the MR signal is exponential and is given by the equation Signal = Soexp (−bD), where So is the attenuation factor, D is the diffusion coefficient of tissue, which characterizes the rates of diffusional motion, and b is the diffusion coefficient factor. The diffusion coefficient is dependent on a number of factors including time, orientation of the imaging plane, tissue being imaged, and the energy state of the imaged tissue [22]. In biologic systems, factors such as perfusion, water transport, or bulk motion might contribute to the signal loss, so that the term apparent diffusion coefficient (ADC) is used instead of diffusion coefficient. The ADC can be calculated on a pixel-by-pixel basis, allowing the generation of a parametric map that reflects the diffusion influence eliminating the T2 effects, which prevents misinterpretation from the so-called T2 shine through effect [21, 22]. Differences in ADC are related to changes in cellularity, cell membrane permeability, intracellular and extracellular diffusion, and tissue structure.

Diffusion-weighted MR imaging is a powerful tool in characterization of brain neoplasms. Tumor cellularity and tumor grade have been correlated with ADC values. Brain neoplasms with higher cellularity or higher grades show a significant reduction in the rate of the ADC and a marked increase in the signal of diffusion-weighted images (Fig.7.5). DWI can also be used in assessing high cellularity of other neoplasms. Lymphoma is a hypercellular tumor that has been found to present with high signal intensity on DWI and low ADC values. Medulloblastoma is a primitive neuro ectodermal tumor that also shows restricted diffusion pattern due to the densely packed cells and high nuclear-to-cytoplasmic ratio. Diffusion-weighted MR images can be used to discriminate the tumor tissue from edema, cyst, or necrosis. The cystic or necrotic portion of the tumor in relation to the normal brain parenchyma appears hypointense on diffusion-weighted images and show much higher ADC values, whereas the areas of enhancing tissue on conventional MRI show high signal intensity on DWI [23–25] (Fig. 2.8).

Atypical and malignant meningiomas also tend to be markedly hyperintense on diffusion-weighted MR images and exhibit lower ADC values, while benign meningiomas have a variable appearance on diffusion-weighted images and higher ADC values compared with normal brain, with the exception of densely calcified or psammomatous meningiomas, which have low ADC values [26].

Diffusion-weighted imaging may also be used to differentiate brain abscess from necrotic or cystic tumor. The abscesses show high signal intensity on DWI and low ADC values due to the presence of the pus, a viscous material that consists of inflammatory cells, debris, and fibrinogen, which leads to reduced water mobility within the cavity [27].

Epidermoid and arachnoid cysts can also be discriminated on the basis of diffusion-weighted images. On conventional spin-echo images, both show long T1 and T2. On diffusion-weighted images, epidermoid cysts show high signal intensity due to restricted motion of protons by the presence of membranes of densely layered epithelium, while arachnoid cysts are hypointense due to their free water motion [28] (Fig. 2.9).

Since diffusion is a 3D process, to acquire more detailed information about anisotropic diffusion properties of the underlying tissue, simple standard DWI is not sufficient. Diffusion tensor imaging (DTI) is a more direct imaging technique to study microarchitecture of brain tissue. Through the application of diffusion sensitization in at least 6 non-colinear directions, it is possible to extract the diffusion tensor and quantify physical parameters like fractional anisotropy or mean diffusivity. Fractional anisotropy reflects the directionality of tissue water diffusion, and therefore, the degree of alignment or integrity of tissue structure within a given voxel (Fig. 2.10a). Mean diffusivity is a measure of overall diffusion in a voxel; its magnitude depends on the total size of extracellular space and the existence of diffusion barriers such as cell membranes or myelin sheaths [29–31] (Fig. 2.10b).

MR DTI allows identification and characterization of white matter tracts according to the direction and degree of their anisotropic water diffusion. Quantifying the degree of anisotropy in terms of metrics such as the fractional anisotropy offers insight into white matter development and degradation. There are fractional anisotropy changes in the white matter of brain neoplasms that might indicate cellular infiltration beyond the area of the tumor enhancement. Within the tumor

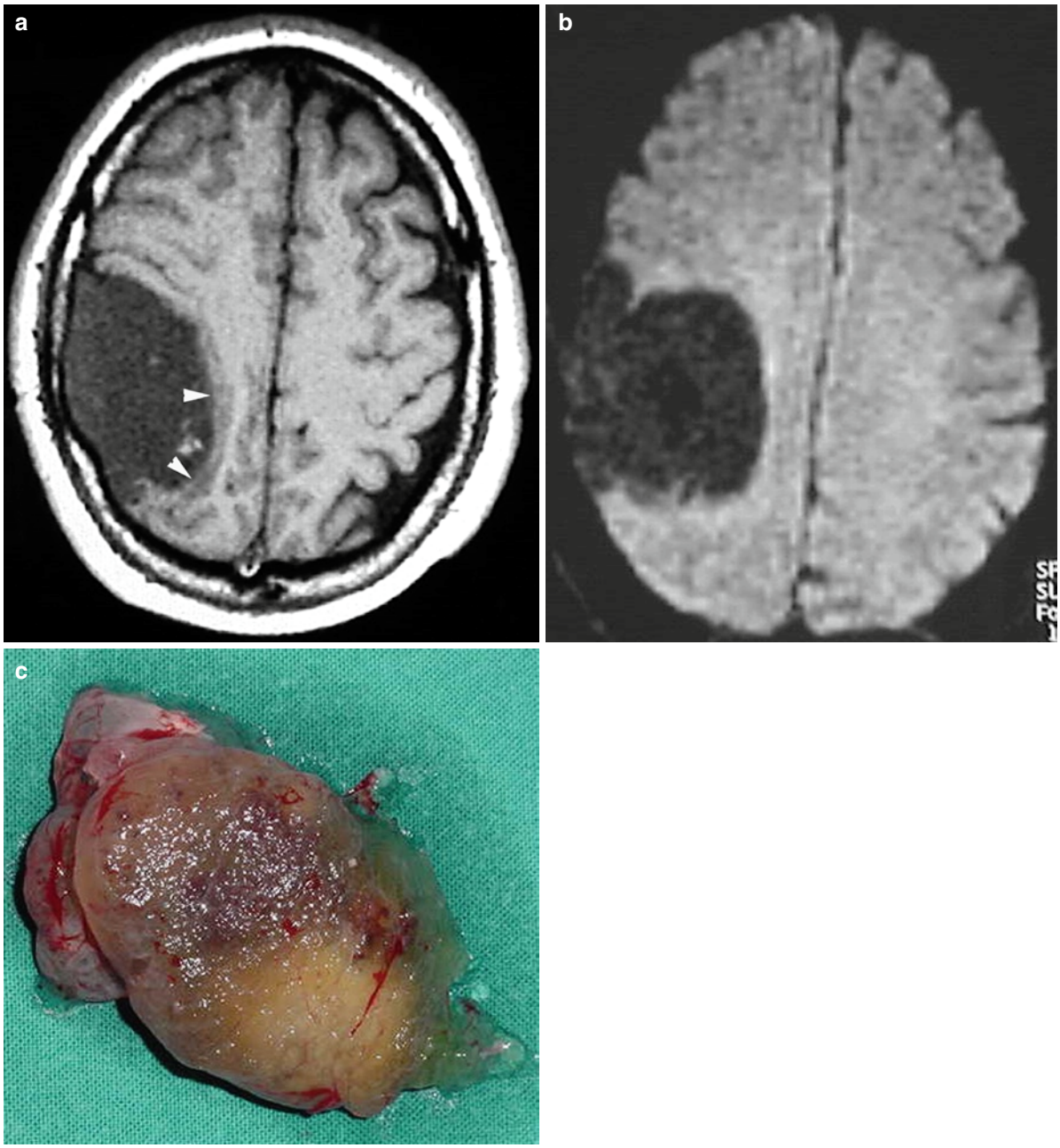

Fig. 2.8 Cystic metastasis. (**a**) T1WI shows a hypointense lesion in the right parietal lobe. The thick capsule of the metastatic lesion is isointense to the gray matter (*arrowheads*). (**b**) On the diffusion-weighted image the lesion is hypointense. (**c**) Gross specimen of the lesion shows a central necrotic area surrounded by a thick capsule

center white matter fibers are displaced by cellular infiltration and fractional anisotropy is reduced, whereas in the periphery and in a narrow rim of white matter rim surrounding the tumor, this parameter could preserve or even increased by fiber compression due to space occupying effect of the tumor [32, 33].

Technical advances in diffusion-weighted imaging enable the assessment of the water diffusivity in 3D space [34, 35]. In vivo, white matter tracts show comparatively higher diffusion anisotropy because water diffusion is more facilitated along the direction of the fibers as compared to diffusion behavior perpendicular

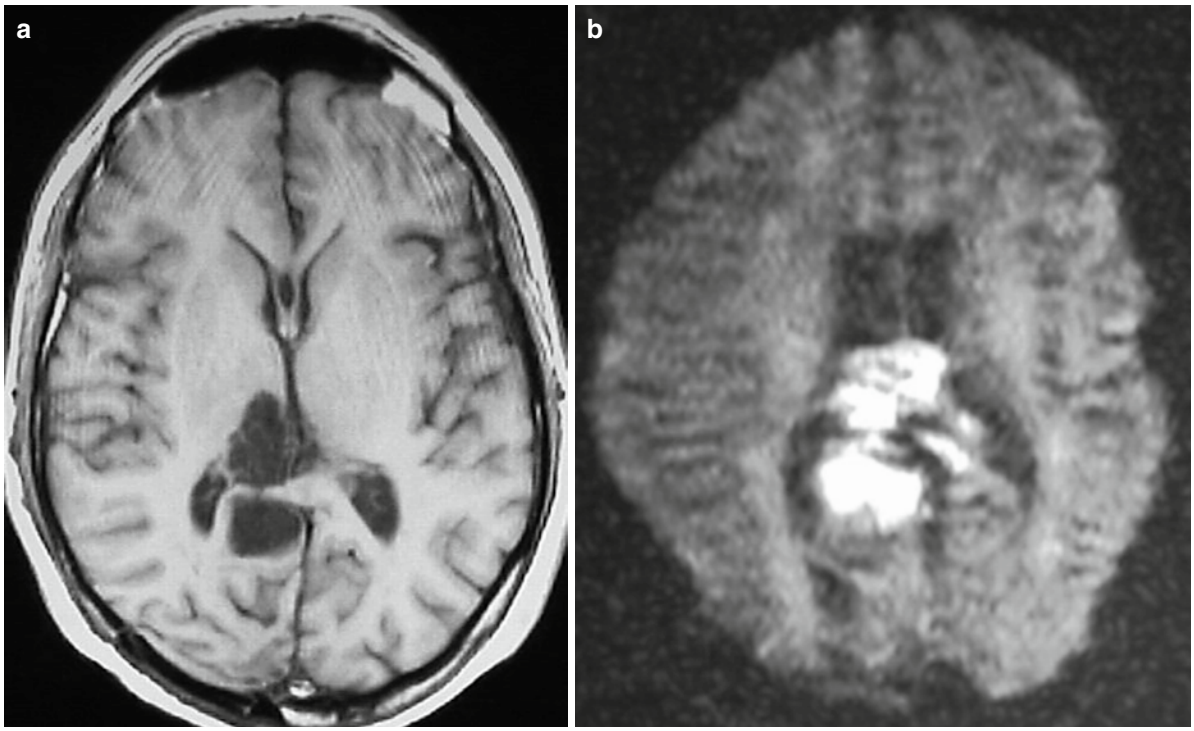

Fig. 2.9 Epidermoid cyst. (**a**) T1WI shows low signal intensity. (**b**) Diffusion-weighted image shows high signal intensity indicative of restricted diffusion

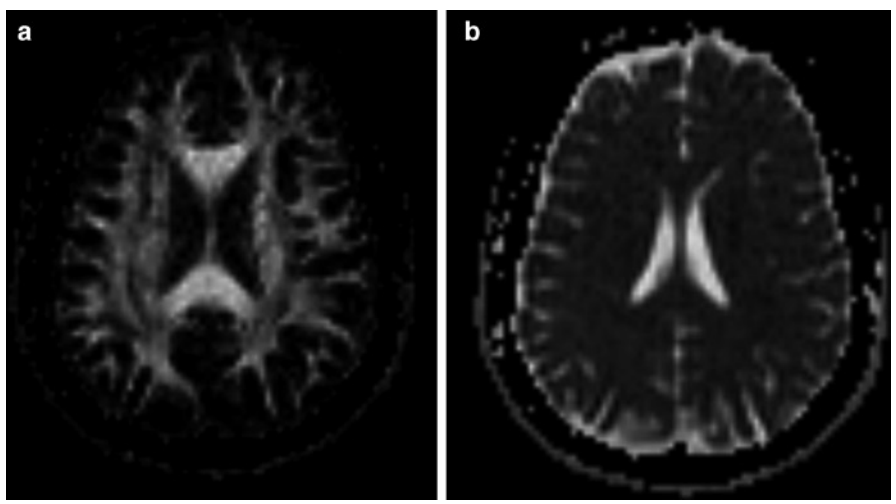

Fig. 2.10 (**a**) Fractional anisotropy map of a normal brain presenting with high signal intensity WM areas of dense myelin like splenium and genu of corpus callosum, while CSF and gray matter exhibit low signal intensity. This can be explained in the basis of local diffusion patterns, where in WM diffusion anisotropy is dominating therefore FA value increases, while in gray matter diffusion becomes isotropic resulting in FA reduction. (**b**) Mean diffusivity of ADC map showing CSF bright due to increased water mobility in fluids, while more solid tissues like gray and white matter presents with significantly lower ADC values

to the fibers [34, 35]. In this context, it is possible to generate 3D representations of the major white matter tracts like corpus callosum (Fig. 2.11). The first step concerning data processing is to estimate each diffusion matrix component values utilizing multiple linear regression methods. The diagonalization of the diffusion tensor provides eigen vectors and eigen values, which correspond respectively to the main diffusion directions and associated diffusivities. Consequently, various indices can be calculated by using combinations of the eigen values. The most commonly used in clinical practice are the mean diffusivity which characterize the mean squared displacement of the water molecules and this parameter is rotationally invariant that means that is independent of the orientation of the reference frame and fractional anisotropy index that describes how much molecular displacements vary in space (ellipsoid eccentricity). In other words, it reflects the degree of alignment of cellular structures within fiber tracts and their structural integrity (Fig. 2.12).

Fig. 2.11 3D representation of the corpus callosum based on diffusion tensor data acquired in 64 directions. The tractography algorithm that was used is the second order Runge–Kutta [55]

Streamline or deterministic fiber tracking algorithms are based on the computation of the eigen system (eigen vectors and their corresponding eigen values) for each voxel. A fiber bundle has a strong anisotropy due to the alignment of the fibers and the local tensors of that bundle have a first eigen value much greater than the others. The diffusion of water protons is most important along the direction first eigen vector (Fig 2.13). Consequently, the detection of strongly anisotropic voxels (based on a threshold value of fractional anisotropy) and representation of the eigen vectors on these voxels can be used to map the white matter fibers since the direction of the first eigen vector is the same with the long axis of the fibers [36]. A major problem of the latter approach is the crossing fibers in the dimensions of a single voxel. In that case, the algorithm fails to delineate two crossing fibers

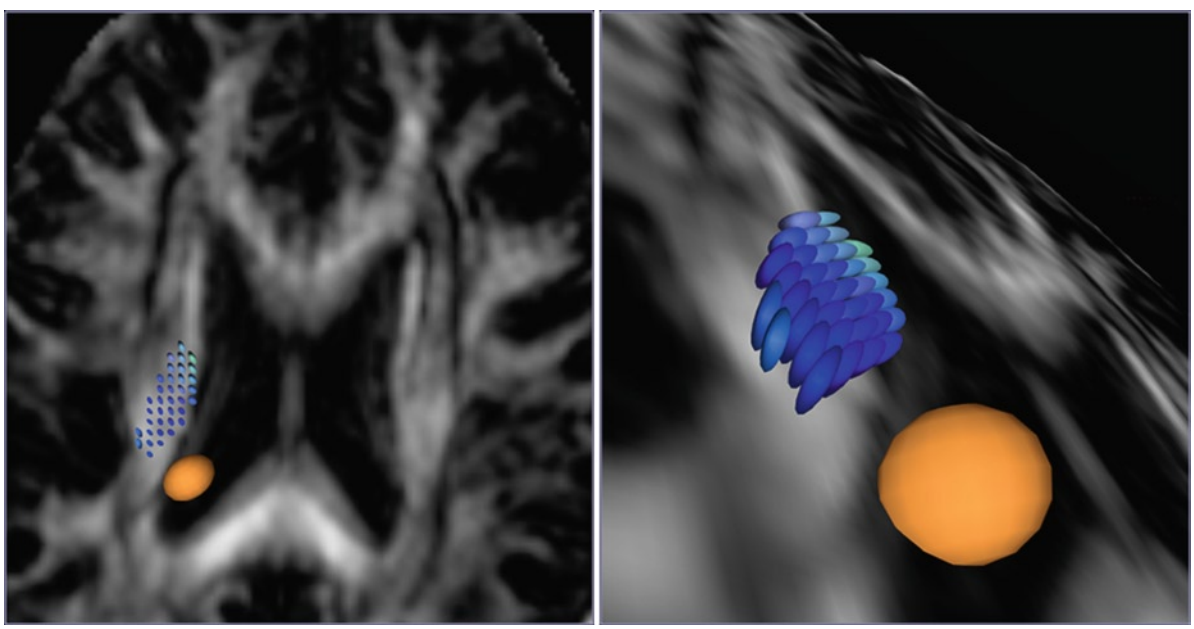

Fig. 2.12 Diffusion properties of CSF can be modeled by almost a sphere due to low anisotropy. On the contrary posterior corona radiata is modeled by elipsoids typical for anisotropic diffusion. Note that the size of either the sphere or the elipsoid represents the value of ADC while the shape represents the type of diffusion, ellipsoid in case of anisotropic diffusion and sphere in case of isotropic diffusion

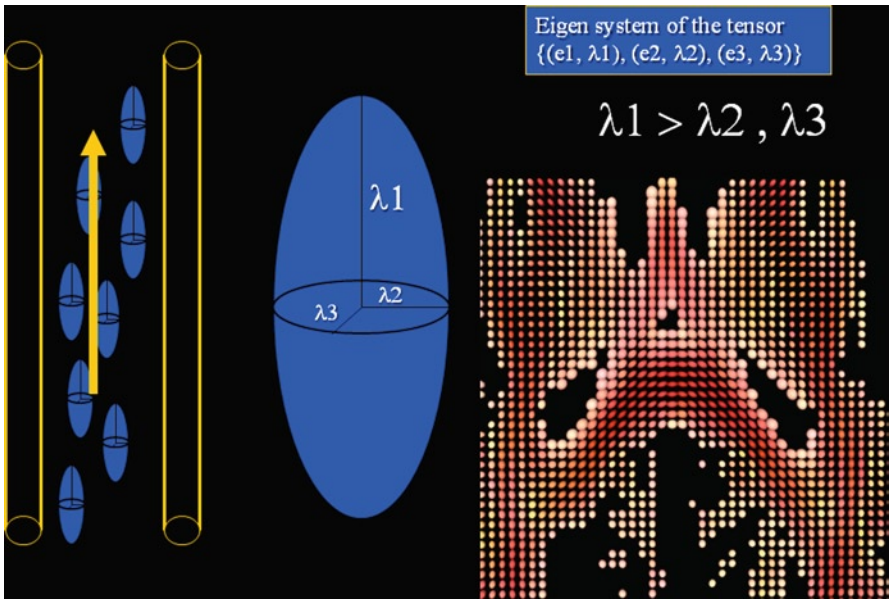

Fig. 2.13 Water mobility is facilitated along the direction of the tracts; therefore the principle diffusion eigenvalue λ1 is considerably higher than the λ2 and λ3 that describe water mobility perpendicular to the fibers

and local errors in the generation of tracts might take place. An alternative strategy to deterministic streamline algorithms is probabilistic tractography. With the latter techniques, it is possible to track fibers in areas of high uncertainty; either these represent areas with low FA values (Fig. 2.14) or areas where crossing of fibers is taking place.

Perfusion-weighted imaging provides information about the perfusion status of microcirculation.

This technique requires the dynamic intravenous administration of a MR contrast agent. As the paramagnetic contrast agent passes through the intravascular compartment local field inhomogeneities are created that result in magnetic susceptibility effects with a decrease in signal on T2*-images that can be measured. This signal drop depends on both the vascular concentration of contrast agent and the concentration of small vessels per voxel tissue [37, 38]. Changes in signal intensity may be used to calculate an image of the relative cerebral blood volume (rCBV). Echo planar MR imaging systems, which use strong rapidly switching magnetic field gradients, permit the fast simultaneous acquisition of multiple T2-weighted slices during the administration of contrast material (Fig. 2.15).

In brain tumor, rCBV maps are particularly sensitive for depicting the microvasculature of a tumor and therefore its aggressiveness and proliferative potential. Previous studies correlating histopathologic grading of gliomas with rCBV showed a positive correlation of rCBV with tumor grading. Especially low-grade gliomas had homogeneous low rCBV, while high-grade tumors exhibited varying degrees of high rCBV [39, 40] (Fig. 4.2).

rCBV maps may also be used to delineate tumor margins as well as to differentiate tumor recurrence from enhancing non-neoplastic tissue such as radiation necrosis which would be useful for surgical planning and targeting of biopsies (Fig. 2.16) and radiation therapy [18] (Fig. 2.17). An enhancing lesion with a normalized rCBV ratio higher than 2.6 or lower than 0.6 may suggest tumor recurrence or non-neoplastic contrast enhancing-tissue, respectively [38, 41].

Perfusion MR may also be used in AIDS patients, to differentiate toxoplasmosis from lymphoma. In toxoplasmosis, the surrounding edema shows vasoconstriction with reduced rCBV, while in lymphomas there are areas with increased cerebral blood volume correlating, with hypervascularity of active neoplastic tissue [42, 43] Conversely, a recent study of perfusion MR imaging in eight patients with lymphoma showed that cerebral lymphomas had a tendency to have low rCBV values [44]. Thus, rCBV mapping may be of limited value in grading lymphoma patients. Finally, perfusion MR imaging may be used in evaluating the pathological changes of chemotherapy in patients with brain tumors.

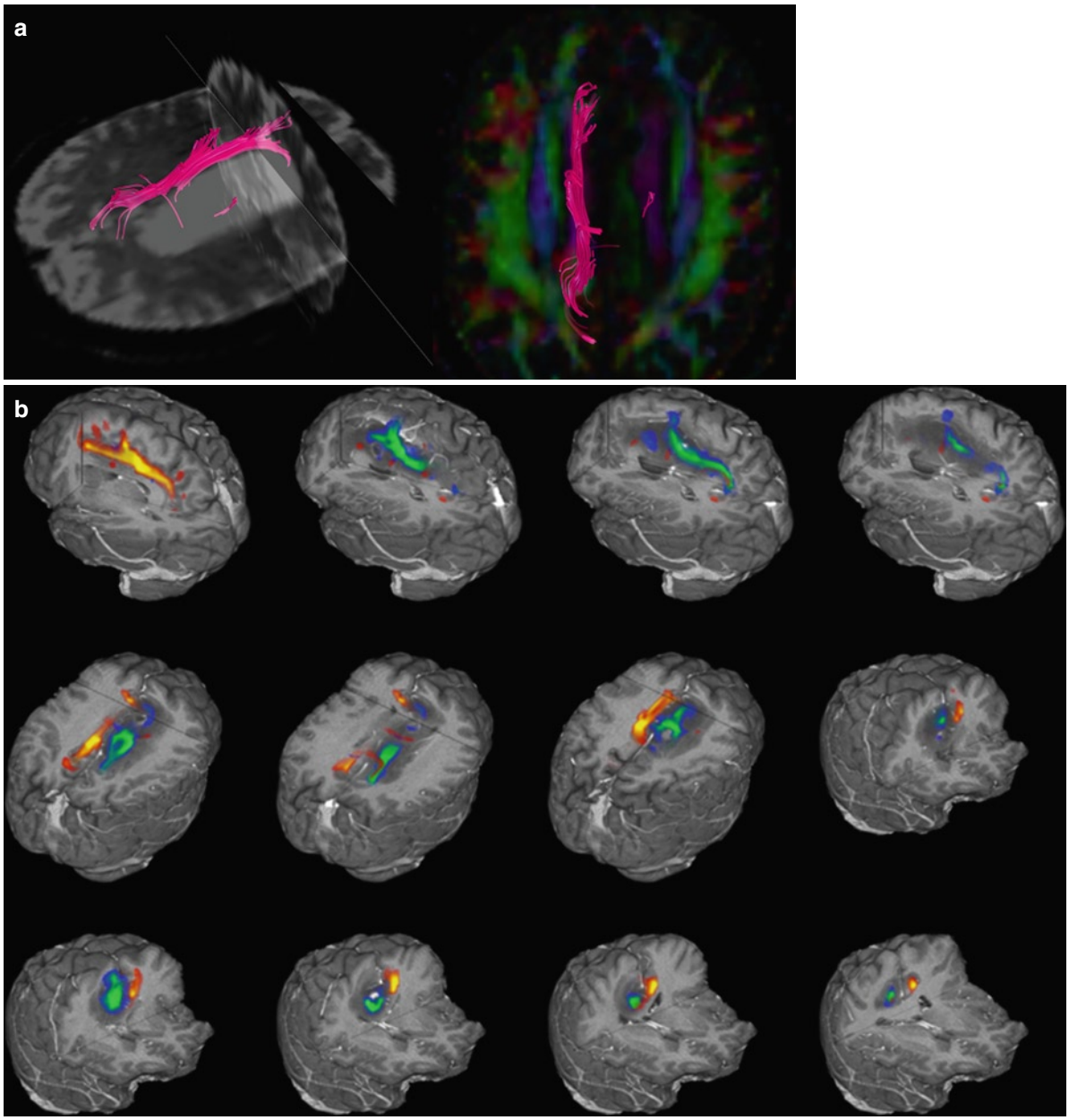

Fig. 2.14 (**a**) Patient with low-grade glioma. Three dimensional representation of cingulate bundles based on deterministic tractography algorithm. The left cingulate is barely seen, most probably, due to lower FA value than the threshold (0.2) utilized by the algorithm to avoid erroneous fiber drawing [55]. (**b**) Probabilistic tractography demonstrate both cingulate bundles. The left cingulate is shown intact but displaced from the tumor [56]

Cortical activity may be studied by fMRI techniques that are mostly based on the detection of the focal blood flow and oxygenation changes following neuronal activity. *The BOLD* effect is the most commonly used to study cortical function in the brain. Neural activation leads to an increase in local blood flow and thus to an increase of oxygenated hemoglobin in the capillaries of activated brain tissue. As a result the oxy/deoxygenated blood ratio is increased. The drop in the concentration of the paramagnetic deoxyhemoglobin leads to a focal signal increase in the affected tissue using T2*-weighted sequences [19, 45]. This effect is

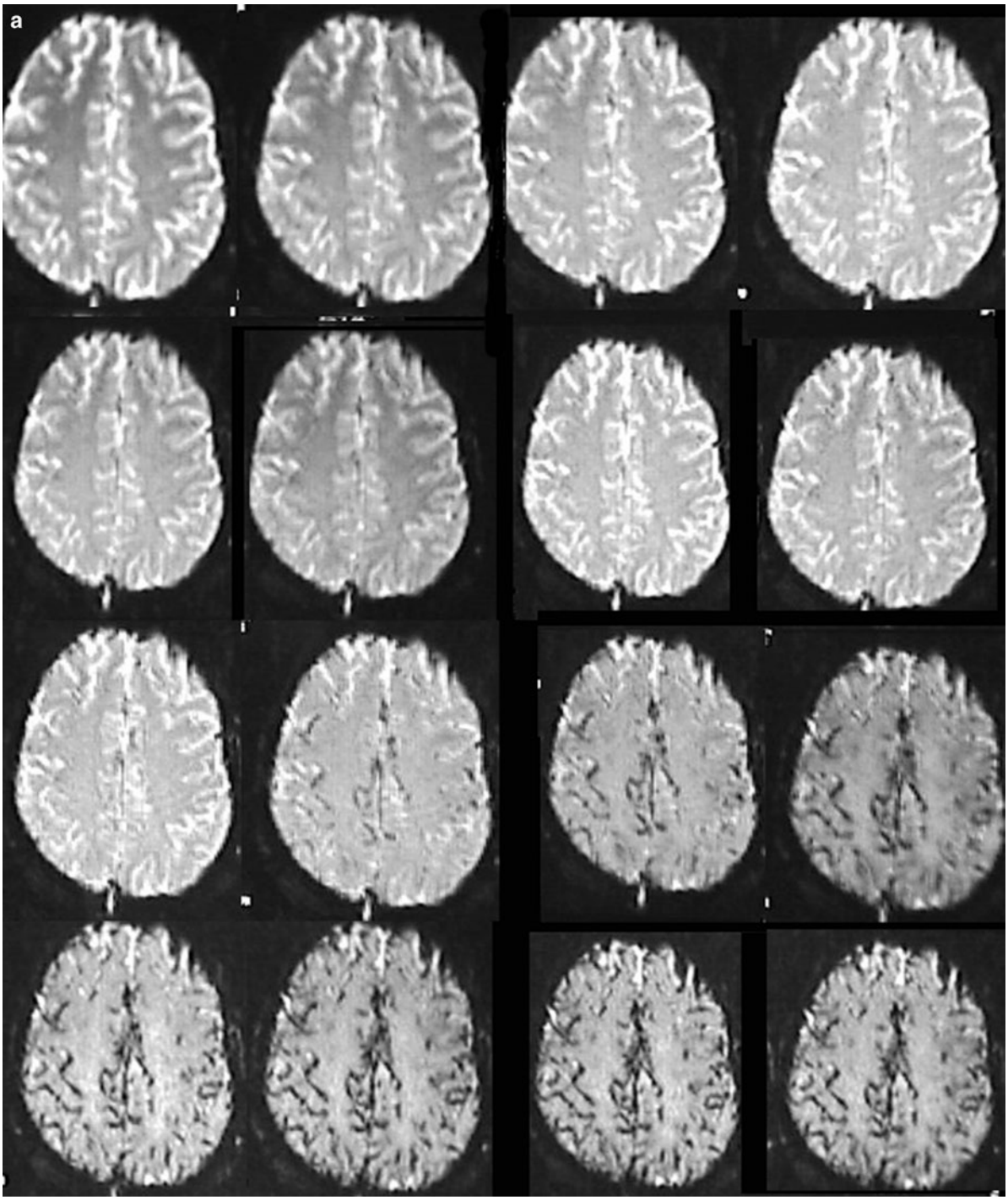

Fig. 2.15 (**a**) Serial echo planar images of the brain during contrast administration. Single slice images with 1 s interval between the images. From left to right the T2 signal intensity is gradually dropped due to the T2* susceptibility effect of gadolinium. (**b**) MR signal versus time curves show signal drop with passage of bolus of contrast material. Upper and lower curves correspond to regions of interest drawn in white and gray matter, respectively. Note greater decrease in signal intensity in gray matter compared with the white matter

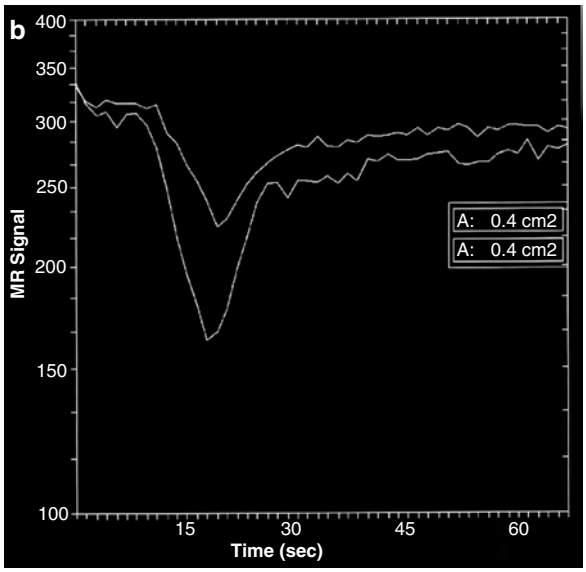

Fig. 2.15 (continued)

known as BOLD effect and was first used to show functionally activated brain regions as result of sensory or motor stimulation [46]. In order to depict the BOLD effect, echo planar sequences must be used due to a very short time window of the BOLD effect and the reduced sensitivity to motion that EPI sequences may provide with. BOLD imaging can be useful for many applications such as: localization of neural activities in the brain, display areas of the brain activate by sensory or motor activation (Fig. 2.18), and as a noninvasive tool for the presurgical mapping of cortical function in patients with intracranial tumors [47–49] (Fig. 2.19). Therefore, functional MRI can contribute to more efficient surgical removal of both benign and malignant brain tumors with an increase in patient survival and a decrease in surgical morbidity [50].

Proton magnetic resonance spectroscopy (1H-MRS) is a noninvasive method to study various chemical compounds found on human brain tissue. It has been demonstrated that this technique provides with biochemical information, which can be useful in differentiating normal from abnormal brain tissue and in a certain extent provide information that might be important for differential diagnosis. Two different approaches have been implemented, namely, single voxel spectroscopy (SVS) and chemical shift imaging

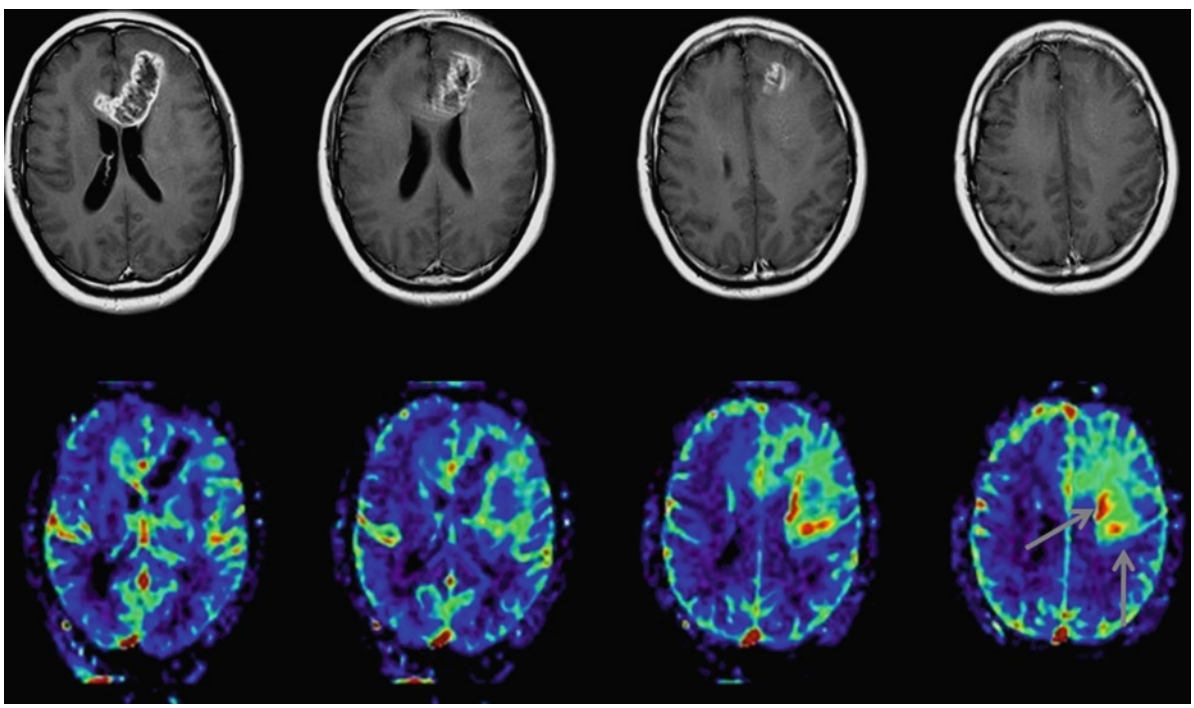

Fig. 2.16 Patient with glioblastoma multiform. In the upper row, a series of postgadolinium T1-,weighted consecutive axial slices showing peripheral enhancement at the genu of corpus callosum. Biopsy guidance can be more accurately performed when rCBV maps are utilized since an area of considerably higher neovascularity is only depicted on rCBV maps (*arrow*)

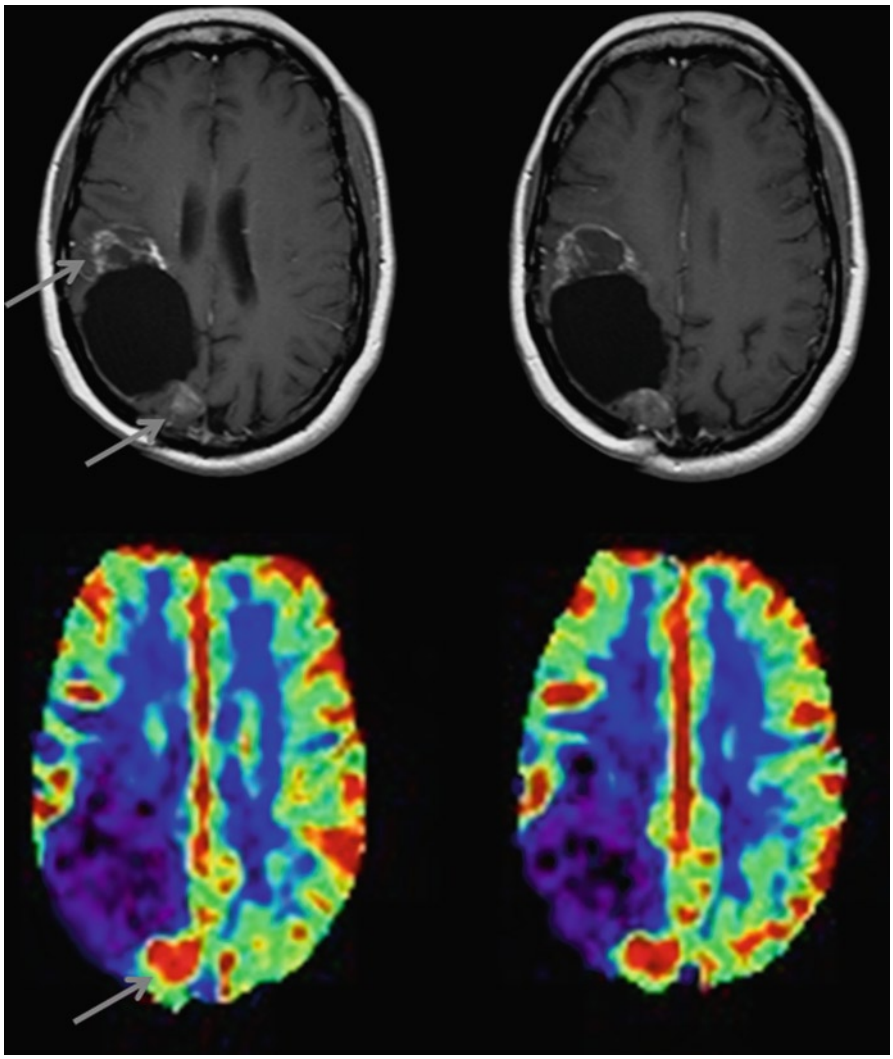

Fig. 2.17 Patient with high-grade glioma after surgery and radiation therapy. Two enhancing areas are shown on postgadolinium T1-weighted axial images (*upper row*, *arrows*). On rCBV maps, the lesion located posterior to the surgical cavity presents with high rCBV value (*red color*) that corresponds to tumor recurrence, while the lesion anteriorly to the surgical cavity is manifested with low rCBV that is compatible with radiation necrosis

(CSI). According to the first, a 3D area or volume of tissues is excited and the signals detected from this volume are transformed to a spectrum. In the second technique, multiple voxels are utilized either in a plane (2D CSI) or in a volume (3D CSI); therefore,it is possible to study larger areas with a single experiment. Metabolic maps can be calculated based on the information derived from each voxel.

SVS produces a single spectrum from a single voxel that is typically 8 cm^3 in volume, whereas CSI measures spectra from multiple voxels that are typically 1–1.5 cm^3 in volume. CSI data may be presented in a variety of displays including individual spectra, spectral maps, or colored metabolite images overlaid on anatomical images (Fig. 2.20).

In MR spectroscopy, different echo time (TE) values can be utilized to control the "T2 contrast" of spectral peaks in the same way tissue T2 contrast is controlled in conventional imaging sequences. Metabolites with short T2 relaxation times decay faster, and the corresponding spectral peaks are not seen on long TE spectra. This type of metabolites can only be detected on short TE acquisitions. The major healthy brain metabolite peaks that are seen on long TE spectra include *N*-acetyl aspartate (NAA) at 2.02 and 2.6 ppm which is a neuronal marker, choline (Cho) at 3.20 ppm which is a membrane marker, and creatine (Cr) at 3.02 and 3.9 ppm which is an energy marker and generally is stable. Short TE spectra contain additional peaks, which include glutamine and glutamate (Glx) between 2.05–2.5 ppm and

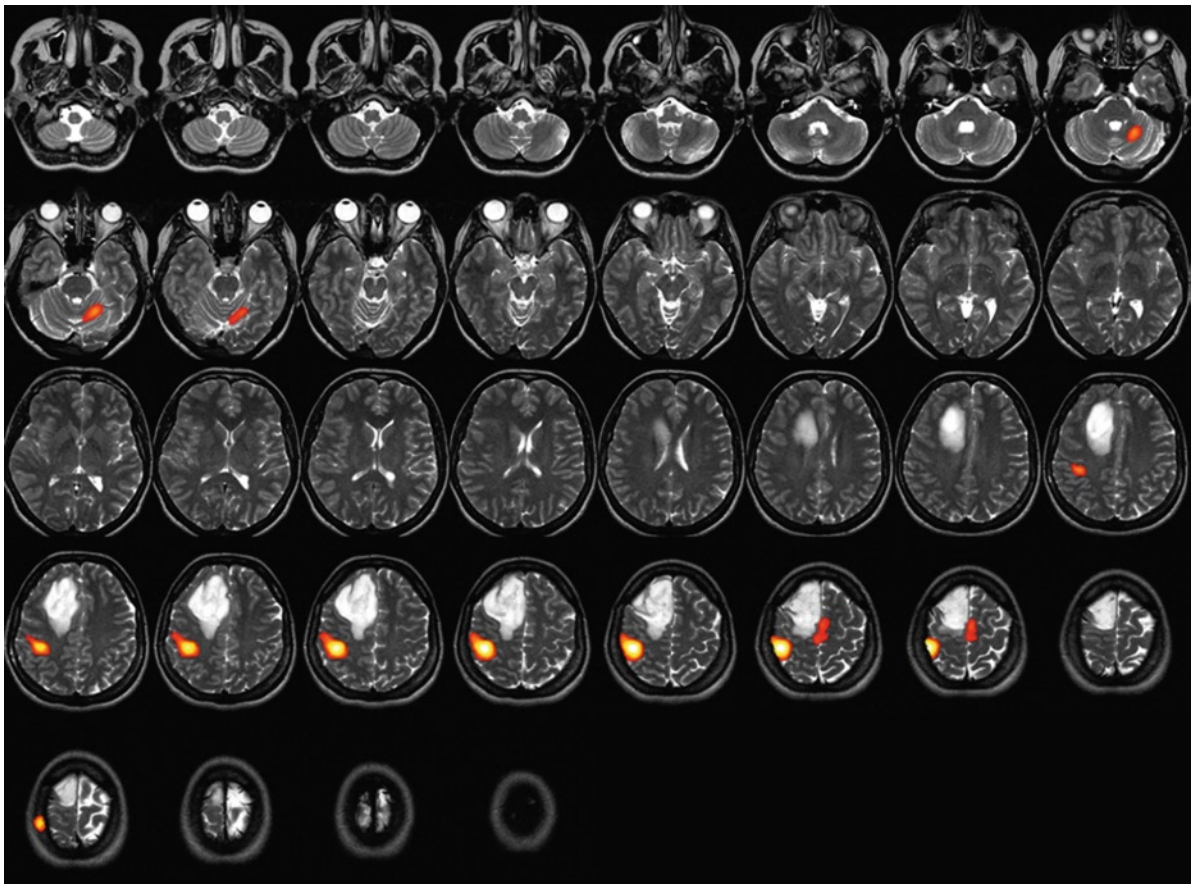

Fig. 2.18 Motor cortex activation during a finger tapping experiment in a patient with a high-grade tumor. Areas of activation are superimposed on axial T2-weighted images

3.65–3.8 ppm, scyllo-inositol (sI) at 3.36 ppm, glucose at 3.43 and 3.8 ppm, and myo-inositol (mI) at 3.56 and 4.06 ppm which is a glial marker.

The most important advantages of SVS over CSI are: (a) shorter acquisition times, (b) better localized shimming, (c) simpler in terms of post-processing and precise volume definition. The most important disadvantage is that SVS can provide spectra only from one voxel and it can be time consuming when multiple, remote areas should be evaluated.

In many disease processes, biochemical changes are preceding morphologic alterations in tissues, therefore MR spectroscopy is a powerful technique to identify early changes comparing to conventional MRI morphologic techniques. As a general rule, brain gliomas show increase of Cho and decrease of NAA peaks compared to normal brain tissue (Fig. 2.21). According to tumor grading the relative Cho/Cr and Cho/NAA ratios show significant increase from low to high-grade gliomas. The most important clinical applications of MR Spectroscopy, either as a stand-alone technique or in combination with diffusion and perfusion weighted imaging techniques, can be summarized into the differentiation between (a) low and high-grade gliomas, (b) radiation induced necrosis and tumor recurrence, (c) primary and secondary malignant tumors and (d) abscesses and tumors. Another important clinical application of MR spectroscopy is the assessment of the therapeutic outcome by performing a baseline evaluation and follow-up experiments to identify therapeutic-induced changes and guide the therapeutic scheme [51–54].

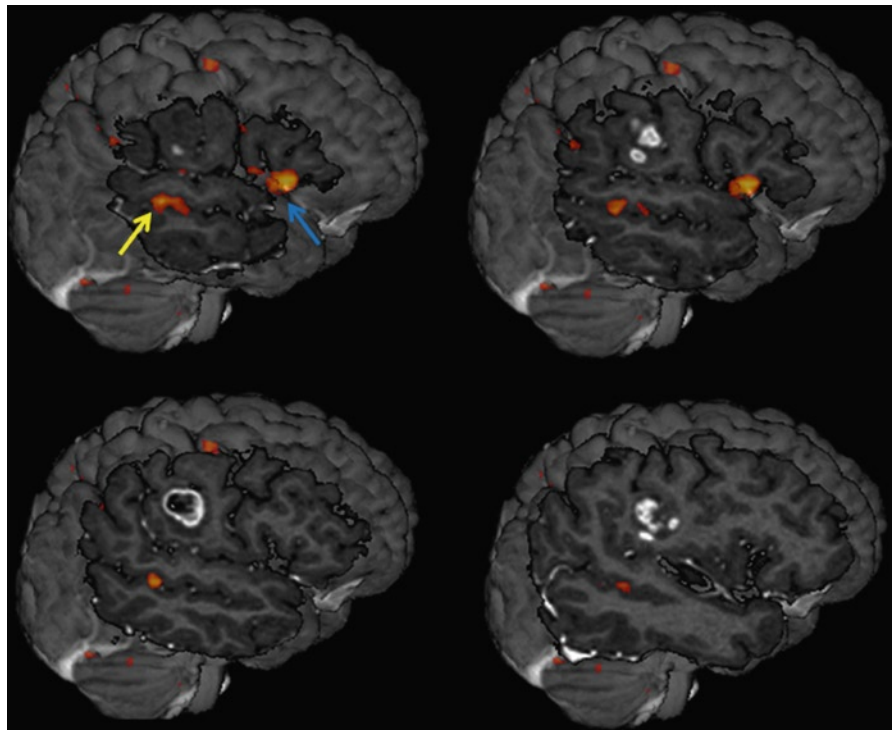

Fig. 2.19 Language centers activation with fMRI in a patient with a high-grade tumor. Activation areas are evident both in Wernicke (*yellow arrow*) and Broca (*blue arrow*) areas

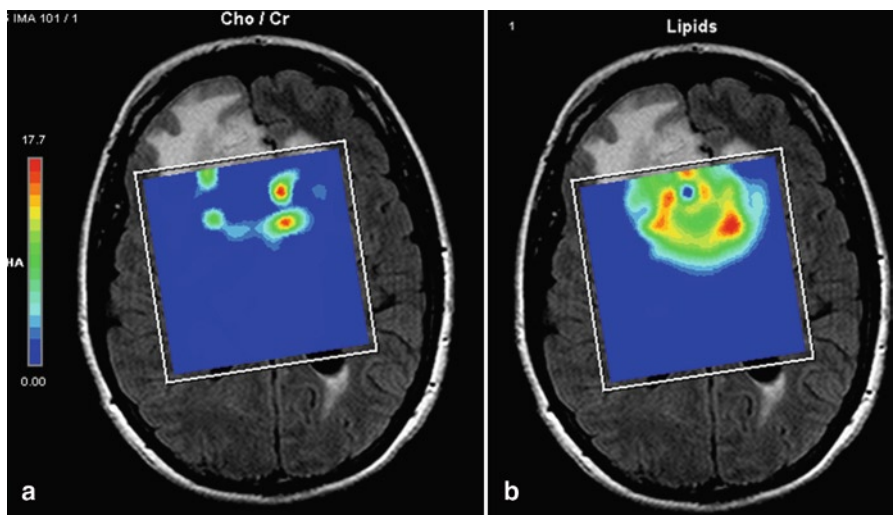

Fig. 2.20 (**a**) Choline (Cho) over creatine and (**b**) lipids metabolite maps generated with chemical shift imaging experiment

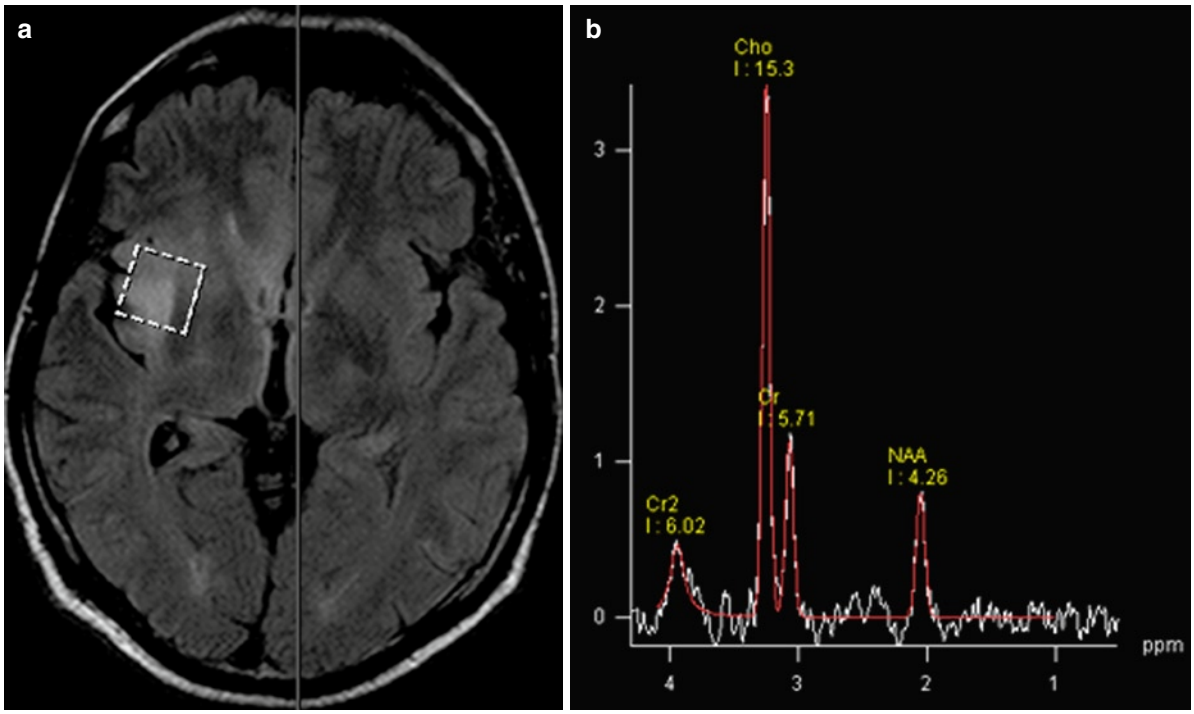

Fig. 2.21 Anaplastic astrocytoma shows high signal intensity on axial FLAIR image (**a**) and elevated choline and reduced NAA on the corresponding spectroscopic image (**b**)

References

1. Nabavi DG, Cenic A, Craen RA et al (1999) CT assessment of cerebral perfusion: experimental validation and initial clinical experience. Radiology 213:141–149
2. Whelan HT, Clanton JA, Wilson RE et al (1988) Comparison of CT and MRI brain tumor imaging using a canine glioma model. Pediatr Neurol 4(5):279–283
3. Runge VM, Kirsch JE, Burke VJ et al (1992) High dose gadoteridol in MR imaging of intracranial neoplasm. J Magn Reson Imaging 2:9–18
4. Yoursy I, Camelio S, Schmid UD et al (2000) Visualization of cranial nerves I-XII: value of 3D CISS and T2 –weighted FSE sequences. Eur Radiol 10(7):1061–1067
5. Yuh WT, Fisher DJ, Engelken JD et al (1991) MR evaluation of CNS tumors: dose comparison study with gadopentate dimeglumine and gatoteridol. Radiology 180:485–491
6. Yuh WT, Fisher DJ, Runge et al (1994) Phase III multicenter trial of high-dose gadoteridol in MR evaluation of brain metastases. AJNR Am J Neuroradiol 15:1037–1051
7. Yuh WT, Nguyen HD, Tali ET et al (1994) Delineation of gliomas with various doses of MR contrast material. AJNR Am J Neuroradiol 15:983–989
8. Abdulach ND, Mathews VP (1999) Contrast issues in brain tumor imaging. Neuroim Clin North Am 9(4):733–749
9. Van Dijk P, Sijens PE, Schmitz PIM et al (1997) Gd-enhanced MR imaging of brain metastases: contrast as a function of dose and lesion size. Magn Reson Imaging 15:535–541
10. Knauth M, Forsting M, Hartmann M (1996) MR enhancement of brain lesions: increased contrast dose compared with magnetization transfer. AJNR Am J Neuroradiol 17:1853–1859
11. Kurki T, Niemi P, Valtonen S (1995) Tissue characterization of intracranial tumors: the value of magnetization transfer and conventional MRI. Neuroradiology 37:515–521
12. Olson EM, Healy JF, Wong WHM et al (1994) MR detection of white matter disease of the brain in patients with HIV infection: fast spin-echo vs conventional spin-echo pulse sequences. AJNR Am J Neuroradiol 162:1199–1204
13. Essig M, Schlemmer HP, Tronnier V et al (2001) Fluid-attenuated inversion recovery MR imaging of gliomatosis cerebri. Eur Radiol 11:303–308
14. Tsuchiya K, Mizutani Y, Hachiya J (1996) Preliminary evaluation of fluid-attenuated inversion-recovery MR in the diagnosis of intracranial tumors. AJNR Am J Neuroradiol 17:1081–1086
15. Essig M, Knopp MV, Schoenberg SO et al (1999) Cerebral gliomas and metastases: assesment with contrast-enhanced fast fluid-attenuated inversion-recovery-imaging. Radiology 210:551–557
16. Westbrook C, Kaut C (1993) Image weighting and contrast. In: Westbrook C (ed) MRI in practise. Blackwell Scientific Publications, pp 17–46
17. Fellner F, Fellner C, Held P et al (1997) Comparison of spin-echo MR pulse sequences for imaging of the brain. AJNR Am J Neuroradiol 18:1617–1625
18. Wong JC, Provenzale JM, Petrella JR (2000) Perfusion MR imaging of brain neoplasms. AJR Am J Roentgenol 174:1147–1157
19. Edelman RR, Wiclopolski P, Schmitt F (1994) Echo-planar MR. Radiology 192:600–612

20. Patel MR, Siewert B, Klufas R et al (1999) Echo planar MR imaging for Ultrafast detection of brain lesions. AJR Am J Roentgenol 173:479–485
21. Sievert B, Patel MR, Mueller MF et al (1995) Brain lesions in patients with multiple sclerosis: detection with echo-planar imaging. Radiology 196:765–777
22. Baird AE, Warach S (1998) Magnetic resonance imaging of acute stroke. J Cereb Blood Flow Metab 18:583–609
23. Nelson SJ, Nat D (1999) Imaging of brain tumors. Neuroimaging Clin N Am 9(4):801–819
24. Okamoto K, Ito J, Ishikawa K et al (2000) Diffusion-weighted echo-planar imaging in the differential diagnosis of brain tumors and tumor-like conditions. Eur Radiol 10(8):1342–1350
25. Sugahara T, Korogi Y, Kochi M et al (1999) Usefulness of diffusion-weighed MRI with echo planar technique in the evaluation of cellularity in gliomas. J Magn Reson Imaging 9(1):53–60
26. Filippi CG, Edgar MA, Ulu AM et al (2001) Appearance of meningiomas on diffusion-weighted images: correlating diffusion constants with histopathologic findings. AJNR Am J Neuroradiol 22:65–72
27. Kim YJ, Chang KH, Song IC et al (1998) Brain abscess and necrotic or cystic brain tumor discrimination with signal intensity on diffusion-weighted MR imaging. AJR Am J Roentgenol 171:1487–1490
28. Tsuruda JS, Chew WM, Moseley ME et al (1990) Diffusion-weighted MR imaging of the brain: value of differentiating between extraaxial cysts and epidermoid tumors Am J Neuroradiol 11:925–931
29. Le Bihan D, Breton E, Lallemand D, Grenier P, Cabanis E, Laval-Jeantet M (1986) MR imaging of intravoxel incoherent motions: application to diffusion and perfusion in neurologic disorders. Radiology 161:401–407
30. Chenevert TL, Brunberg JA, Pipe JG (1990) Anisotropic diffusion in human white matter: demonstration with MR techniques in vivo. Radiology 177:401–405
31. Basser PJ, Pierpaoli C (1996) Microstructural and physiological features of tissues elucidated by quantitative-diffusion-tensor MRI. J Magn Reson B 111(3):209–219
32. Maier SE, Mamata H (2008) Diffusion Imaging of Brain Tumors. In: Newton EB, Jolesz FA (eds) Handbook of neurooncology neuroimaging. Academic Press, Elsevier, pp 239–247
33. Celso Hygino Cruz L Jr, Domingues RC, Sorensen AG (2008) Diffusion Magnetic Resonance Imaging in Brain Tumors. In: Newton EB, Jolesz FA (eds) Handbook of neurooncology neuroimaging. Academic Press, Elsevier, pp 215–238
34. Basser PJ, Pajevic S, Pierpaoli C, Duda J, Aldroubi A (2000) In vivo fiber tractography using DT-MRI data. Magn Reson Med 44(4):625–632
35. Catani M, Howard RJ, Pajevic S, Jones DK (2002) Virtual in vivo interactive dissection of white matter fasciculi in the human brain. Neuroimage 17(1):77–94
36. Mori S, Crain BJ, Chacko VP, van Zijl PCM (1999) Three dimensional tracking of axonal projections in the brain by magnetic resonance imaging. Ann Neurol 45:265–269
37. Baird AE, Benfield A, Schlaug G et al (1997) Enlargement of human cerebral ischemic lesion volumes measured by diffusion-weighted magnetic resonance imaging. Ann Neurol 41:581–589
38. Demaerel PH (ed) (2000) Recent advances in diagnostic neuroradiology. Springer Verlag, Berlin, pp 119–135
39. Aromen JH, Gazit IE, Louis DN et al (1994) Cerebral blood volume maps of gliomas: comparison with tumor grade and histologic findings. Radiology 191:41–51
40. Roberts HC, Roberts TPL, Brasch RC et al (2000) Quantitavive measurement of microvascular permeability in human brain tumors achieved using dynamic contrast-enhanced MR imaging: correlation with histologic grade. AJNR Am J Neuroradiol 21:891–899
41. Sugahara T, Korogi Y, Tomiguchi S et al (2000) Posttherapeutic intraaxial brain tumor: the value of perfusion sensitive contrast-enhanced MR imaging for differentiating tumor recurrence from nonneoplastic contrast-enhancing tissue. AJNR Am J Neuroradiol 21:901–909
42. Miszkiel KA, Waldan AD (2000) Imaging in AIDS. In: Demaerel PH (ed) Recent advances in neuroradiology. Springer-Verlag, pp 249–273
43. Ernst TM, Chang L, Witt MD et al (1998) Cerebral toxoplasmosis and lymphoma in AIDS: perfusion MR imaging experience in 13 patients. Radiology 208:663–669
44. Sugahara T, Korogi Y, Shigematsu Y et al (1999) Perfusion sensitive MRI of cerebral lymphomas:a preliminary report. J Comput Assist Tomogr 23(2):232–237
45. Sunaert S, Dymarkowski S, Van Oostende S et al (1998) Functional magnetic resonance imaging (fMRI) visualizes the brain at work. Acta Neurol Belg 98:8–16
46. Kwong KK, Belliveau JW, Chesler DA et al (1992) Dynamic magnetic resonance imaging of human brain activity during primary sensory stimulation. Proc Natl Acad Sci 29:5675–5679
47. Mueller WM, Yetkin FZ, Hammeke TA et al (1996) Functional MRI mapping of the motor cortex in patients with cerebral tumors. Neurosurgery 39:515–520
48. Schreiber A, Hubbe U, Ziyeh S et al (2000) The influence of gliomas and non-glial space-occupying lesions on blood-oxygen-level-dependent contrast enhancement. AJNR Am J Neuroradiol 21:1055–1063
49. Shuber M, Maldjian JA, Liu WC et al (1998) Functional image-guided surgery of intracranial tumors located in or near the sensorimotor cortex. J Neurosurg 89:412–448
50. Wilms G, Sunaert S, Flamen P (2000) Recent developments in brain tumor diagnosis. In: Demaerel PH (ed) Recent advances in diagnostic neuroradiology. Springer Verlag, Berlin, pp 119–135
51. Weybright P, Sundgren PC, Maly P, Hassan DG, Nan B, Rohrer S, Junck L (2005) Differentiation between brain tumor recurrence and radiation injury using MR spectroscopy. AJR Am J Roentgenol 185(6):1471–1476
52. Lichy MP, Bachert P, Henze M, Lichy CM, Debus J, Schlemmer HP (2004) Monitoring individual response to brain-tumour chemotherapy: proton MR spectroscopy in a patient with recurrent glioma after stereotactic radiotherapy. Neuroradiology 46(2):126–129
53. Howe FA, Barton SJ, Cudlip SA, Stubbs M, Saunders DE, Murphy M, Wilkins P, Opstad KS, Doyle VL, McLean MA, Bell BA, Griffiths JR (2003) Metabolic profiles of human brain tumors using quantitative in vivo 1H magnetic resonance spectroscopy. Magn Reson Med 49:223–232
54. Moller-Hartmann W, Herminghaus S, Krings T, Marquardt G, Lanfermann H, Pilatus U, Zanella FE (2002) Clinical application of proton magnetic resonance spectroscopy in the diagnosis of intracranial mass lesions. Neuroradiology 44:371–378
55. Wang R, Wedeen VJ (2007) ISMRM abstract. Proc Intl Soc Mag Reson Med 15:3720
56. Woolrich MW, Jbabdi S, Patenaude B, Chappell M, Makni S, Behrens T, Beckmann C, Jenkinson M, Smith SM (2009) Bayesian analysis of neuroimaging data in FSL. Neuroimage 45:S173–S186

http://www.springer.com/978-3-540-87648-9

Imaging of Brain Tumors with Histological Correlations
Drevelegas, A. (Ed.)
2011, X, 440 p. 865 illus., 165 illus. in color., Hardcover
ISBN: 978-3-540-87648-9